
SyNDock: N Rigid Protein Docking via Learnable Group Synchronization

Yuanfeng Ji¹, Yatao Bian^{2*}, Guoji Fu³, Peilin Zhao², Ping Luo^{1*}

¹ The University of Hong Kong

² Tencent AI Lab ³ National University of Singapore

Abstract

The regulation of various cellular processes heavily relies on the protein complexes within a living cell, necessitating a comprehensive understanding of their three-dimensional structures to elucidate the underlying mechanisms. While neural docking techniques have exhibited promising outcomes in binary protein docking, the application of advanced neural architectures to multimeric protein docking remains uncertain. This study introduces SyNDock, an automated framework that swiftly assembles precise multimeric complexes within seconds, showcasing performance that can potentially surpass or be on par with recent advanced approaches. SyNDock possesses several appealing advantages not present in previous approaches. Firstly, SyNDock formulates multimeric protein docking as a problem of learning global transformations to holistically depict the placement of chain units of a complex, enabling a learning-centric solution. Secondly, SyNDock proposes a trainable two-step SE(3) algorithm, involving initial pairwise transformation and confidence estimation, followed by global transformation synchronization. This enables effective learning for assembling the complex in a globally consistent manner. Lastly, extensive experiments conducted on our proposed benchmark dataset demonstrate that SyNDock outperforms existing docking software in crucial performance metrics, including accuracy and runtime. For instance, it achieves a 4.5% improvement in performance and a remarkable millionfold acceleration in speed.

1 Introduction

Protein complexes serve as vital components in numerous biological processes, regulating the expression of essential functions like DNA transcription [1], mRNA translation [2], and signal transduction [3]. Remarkably, experimental evidence has shown that these functions depend not only on binary complexes but also on the involvement of multimeric complexes. Structural information about complexes provides critical insight to understand protein function, cellular components, and mechanisms, aiding biomedical research in identifying drug targets, designing therapies, and advancing our knowledge of diseases. However, the process of detecting the structures of multimeric protein complexes using experimental techniques

such as X-ray diffraction [4] is often characterized by slowness, high cost, and increased technical challenges compared to solving the structures of single protein chains. Therefore, the advancement of

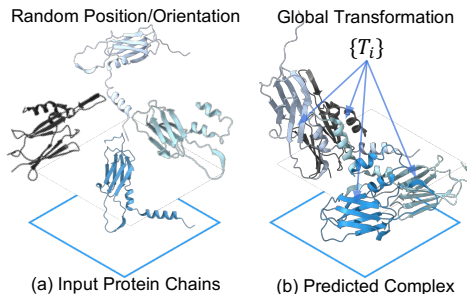


Figure 1: **Task illustration:** (a) Input multiple proteins and (b) the predicted N-body complex structure.

*Corresponding authors: pluo@cs.hku.hk, yatao.bian@gmail.com

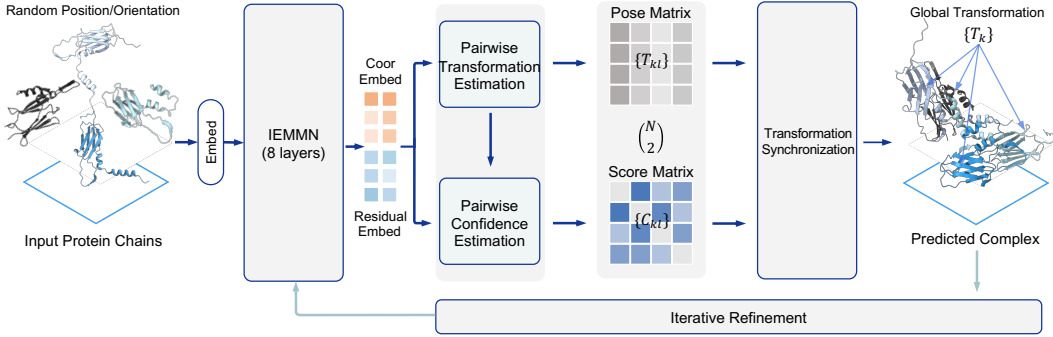


Figure 2: **Overview of SyNDock**, which comprises three main components: (a) The IEMMN backbone models proteins as graphs and extracts feature embeddings. (b) The pairwise pose estimation module and confidence estimation module utilize the feature embeddings to estimate relative transformations and docking confidence scores between protein pairs. (c) The transformation synchronization module combines these predictions in a learnable manner to recover absolute transformations. The prediction of the multimeric complexes can be easily recovered by applying affine transformations.

computational methods for predicting the docking of multimeric protein complexes is of immense importance and offers significant benefits to biomedical research.

Research on the computational prediction of protein complex structures has been conducted for several decades. Most popular docking software [5, 6, 7, 8, 9, 10, 11, 12] is typically limited to the assembly of two protein structures (also known as pairwise docking), and only a few methods [13, 14, 15, 16] can solve multimeric protein docking, although some of them with many restrictions (i.e., homomeric, symmetric). Specifically, these algorithms largely follow the steps of coarsely generating a large number (e.g., millions) of possible pairwise docking candidates, followed by combining pairwise solutions using a combinatorial optimization algorithm (e.g., heuristic or genetic algorithm), and further fitting and refining the top-ranked complex structures based on an energy model (e.g., Monte Carlo [17]). However, all of these methods are still computationally expensive and often take between hours and days to predict, with no guarantee of accurately finding complex structures.

In this paper, we address the problem of *N rigid protein docking*, which refers to predicting the 3D structure of a multimeric complex from the unbound states of individual proteins (Figure 1). This problem assumes that the proteins remain rigid during the docking process, without undergoing any deformation, which is a reasonable and widely applicable assumption in various biological contexts. As an effective solution, we propose SyNDock, a novel learning-centered approach to multimeric protein docking. Our method formulates the problem as learning global $SE(3)$ transformations for each input protein to recover the exact placement and orientation of protein units within the target complex. The pipeline of SyNDock, as shown in Figure 2, consists of several steps. First, a graph-based deep model called the Independent $SE(3)$ -Equivariant Multi-graph Matching Network (IEMMN) extracts informative features from the protein chains. Next, the relative transformations between pairs of protein chains are estimated, along with the corresponding confidence values. Finally, a differentiable transformation synchronization module learns to refine the relative transformations to obtain accurate absolute transformations under the "self-consistent" constraint, overcoming potential noise in the input estimations. These modules are interconnected and trained in an end-to-end fashion and can be iterated to improve performance.

In summary, this paper has three main **contributions**. First, we formulate multimeric protein docking as a problem of learning global transformations to place chain units of a complex, we propose the first end-to-end solution, and it opens a new perspective on multimeric complex docking. Second, we present a carefully designed, fast, and end-to-end two-step pipeline that enables effective learning to assemble the complex in a globally consistent manner. Third, we contribute a hetero-multimeric complex dataset curated from the DIPS dataset [18]. Extensive experiments show that SyNDock outperforms recent advanced methods in both accuracy and speed. For example, SyNDock achieves a 4.5% performance improvement and a millionfold speedup over Multi-Zerd [17] on the tetrameric protein docking task. These contributions collectively demonstrate the effectiveness and practicality of our approach in advancing the field of multimeric protein docking.

2 Related Work

Protein Structure Prediction. Recently, the deep learning based methods AlphaFold2 [19] and Rosettafold [20] have made a profound impact on the field of structural biology [21]. These methods have enabled the prediction of protein structure from primary amino acid sequences and have demonstrated a promising avenue for the tertiary structure determination of proteins. Inspired by the success of these two methods, there have been several attempts to use pre-trained AlphaFold2 to predict the structure of protein complexes [22, 23, 24] by inserting a linker between two isolated protein sequences. These methods rely on the slow construction of multiple sequence alignment (MSA) features and are often unable to handle complex docking tasks involving more than two chains.

Protein-Protein Docking. Classical experimental methods for determining the structure of protein complexes, including X-ray crystallography [25, 26], nuclear magnetic resonance spectroscopy (NMR) [27, 28], and cryogenic electron microscopy (Cryo-EM) [29, 30, 31]. However, such assays are laborious and expensive, and researchers are trying to solve this problem with computational methods. As a focal point of activity in computational and structural biology, structure-based docking approaches [32] are attracting great research interest [33, 34, 35, 36, 37, 38, 39, 40, 41, 42]. They are mainly designed to solve the assembly of paired protein structures, also known as pairwise docking, which typically consists of several main steps: sampling a large number of candidate protein complexes and ranking these candidates with a score function. Finally, the top candidates are further refined using energy or geometric models [43]. Recently, EquiDock [44] proposed an end-to-end rigid pairwise protein docking method that is free of the candidate sampling constraint and thus greatly accelerates prediction. Despite the observed steady progress in the field, methods for assembling three or more chains have received less attention. The pioneering work [45, 17] enabled the assembly of multimeric proteins by using optimal combination algorithms from pairwise docked candidates generated by standard binary docking methods. A series of subsequent papers [14, 15] made improvements in various aspects to achieve even better performance. However, these methods follow the classic paradigm of sampling a large number of complex candidates and further optimizing them using hand-crafted geometric or chemical features to obtain the final structure, resulting in inefficient predictions and unsatisfactory performance.

Transformation Synchronization. Given a collection of pairwise estimates, synchronization seeks to synchronize and recover the absolute estimates of latent values that best explain them. In this paper, we focus on transformation synchronization, which is applicable to both $SO(3)$ and $SE(3)$. For docking multimeric proteins, one could naively consider only adjacent protein pairs and aggregate the transformations sequentially. However, this only works if all pairwise estimates are accurate, and an inaccurate/non-existent pairwise alignment will cause the result to fail. Various approaches have been proposed to more accurately determine the optimal global transformation by considering the additional information contained in the relative transformation, such as the level of confidence. The method of [46, 47] proposes a closed-form solution for $SO(3)$ and $SE(3)$ synchronization based on the eigendecomposition of a weighted pairwise transformation matrix. The following approaches [48, 49] build on these ideas and integrate transformation synchronization with a supervised end-to-end multi-view point cloud registration pipeline. We extend transformation synchronization for the first time to effectively and efficiently predict the structure of multimeric protein complexes.

3 Preliminaries and Background

Problem Statement We consider a set of N potentially interacting proteins $\mathcal{S} = \{\mathcal{G}_k\}_{k=1}^N$ as input, which forms a multimeric complex. Each protein \mathcal{G}_k consists of n_k residues, represented in their bound (docked) state as 3D point clouds $\mathbf{X}_k^* \in \mathbb{R}^{3 \times n_k}$, where the position of each residue is given by the coordinate of its corresponding α carbon atom. In the unbound state, each undocked protein is arbitrarily rotated and translated in space, resulting in a point cloud $\mathbf{X}_k \in \mathbb{R}^{3 \times n_k}$ with modified random positions and orientations. Given arbitrary proteins and their unbound positions \mathbf{X}_k as input, the rigid protein docking task seeks to calculate the absolute transformations \mathbf{T}_k such that the result of the affine transformation $\mathbf{X}_k \otimes \mathbf{T}_k$ is equal to the desired result \mathbf{X}_k^* . Intuitively, we represent a transformation $\mathbf{T} \in SE(3)$ by a 4×4 matrix. Unless otherwise noted, we denote the rotation and translation components of \mathbf{T} as $\mathbf{R} \in SO(3) \subset \mathbb{R}^{3 \times 3}$ and $\mathbf{t} \in \mathbb{R}^3$ respectively. Rather than regressing the global transformations directly, we first estimate the pairwise transformations $\mathbf{T}_{k,l}$ for each pair of

proteins k and l , and subsequently exploit transformation synchronization to infer the optimal global transformations \mathbf{T}_k accurately. Please refer to the Table 5 in Appendix A for the comprehensive notation of the paper.

Equivariance and Invariance To achieve a reliable prediction of the complex structure, we need to satisfy two constraints: (1) *equivariance constraint*: We desire the predicted structure of the proteins to be independent of their initial positions, orientations, and order of input. (2) *invariance constraint*: We require the final complex structure to be the same after superposition, regardless of the random transformations that are applied. Formally, we wish to guarantee that:

Definition 3.1 (Equivariance). Let $\mathbf{T}_g : \mathcal{X} \mapsto \mathcal{Y}$ be a set of transformations on \mathcal{X} for the abstract group $g \in G$. We say that a function $\phi : \mathcal{X} \mapsto \mathcal{Y}$ is equivariant to g if there exists an equivalent transformation on its output space: $S_g : \mathcal{Y} \mapsto \mathcal{Y}$ such that $\phi(\mathbf{T}_g(\mathbf{x})) = S_g(\phi(\mathbf{x}))$.

Definition 3.2 (Rotation Equivariance). We say that a function ϕ is rotation equivariant if for any orthogonal matrix $\mathbf{Q} \in \mathbb{R}^{3 \times 3}$, rotating the input \mathbf{X} resulting in an equivalent rotation of the output $\phi(\mathbf{X})$, i.e., $\mathbf{Q}\phi(\mathbf{X}) = \phi(\mathbf{Q}\mathbf{X})$.

Definition 3.3 (Translation Equivariance). We say that a function ϕ is translation equivariant if for any translation vector $\mathbf{g} \in \mathbb{R}^3$, translating the input \mathbf{X} by \mathbf{t} results in an equivalent translation of the output $\phi(\mathbf{X})$, i.e, let $\mathbf{X} + \mathbf{g} := (\mathbf{x}_1 + \mathbf{g}, \dots, \mathbf{x}_n + \mathbf{g})$, we have $\phi(\mathbf{X}) + \mathbf{g} = \phi(\mathbf{X} + \mathbf{g})$.

Definition 3.4 ($SE(3)$ -Equivariance). We say that a function ϕ is $SE(3)$ -equivariant if it is translation equivariant and rotation equivariant.

Definition 3.5 (Permutation Equivariance). We say that a function ϕ is permutation equivariant if for any column index permutation operator σ , permuting the input \mathbf{X} results in the same permutation of the output i.e., $\sigma(\phi(\mathbf{X})) = \phi(\sigma(\mathbf{X}))$.

Definition 3.6 (Invariance). Let $\mathbf{T}_g : \mathcal{X} \mapsto \mathcal{Y}$ be a set of transformations on \mathcal{X} for the group $g \in G$. We say that a function $\phi : \mathcal{X} \mapsto \mathcal{Y}$ is invariant to g if $\phi(\mathbf{X}) = \phi(\mathbf{T}_g(\mathbf{X}))$.

4 SyNDock

Overview The overall structure of SyNDock is outlined in Figure 2, which begins by training an encoder Φ network, represented by a graph neural network (GNN) that is $SE(3)$ equivariant, to extract features from N given protein chains \mathcal{S} . Then, the pairwise relative transformations $\{\mathbf{T}_{k,l}\}_{k=1,k \neq l}^N$ between the $\binom{N}{2}$ pairs of protein chains are estimated along with the corresponding confidence values $\{c_{k,l}\}$, and the predicted relative parameters are then synchronized to recover the global absolute transformation $\{\mathbf{T}_k\}_{k=1}^N$ for each of the individual proteins. This overall procedure can be further refined through an iterative process, allowing for incremental improvements in the results. We provide the implementation details in Algorithm 2 in Appendix B for better clarity.

Protein Representation Following the work of [50, 44], we encode each input protein as a 3D proximity graph, and the graph of protein k is denoted as $\mathcal{G}_k = (\mathcal{V}_k, \mathcal{E}_k)$, where each node $i \in \mathcal{V}_k$ corresponds to an amino acid with scalar and vector features of $\mathbf{h}_i \in \mathbb{R}^{f_1}$ and position $\mathbf{x}_i \in \mathbb{R}^3$ corresponding to the Cartesian coordinate of the α carbon atom. An edge $(i, j) \in \mathcal{E}_k$ exists if vertex j is one of the ten most similar neighbors of vertex i based on the Euclidean distance of the coordinates of the two vertices. Each (i, j) also has edge features that encode both scalar and vector features. To satisfy the equivariance constraint, we use the $SE(3)$ -invariant feature engineering proposed by [44] to construct the additional features $\mathbf{f}_i \in \mathbb{R}^{f_2}$ and $\mathbf{f}_{j \rightarrow i} \in \mathbb{R}^{f_3}$ of each node $i \in \cup_{k=1}^N \mathcal{V}_k$ and each edge $(i, j) \in \cup_{k=1}^N \mathcal{E}_k$, respectively. For more details on protein encoding and feature engineering, please refer to Appendix B.

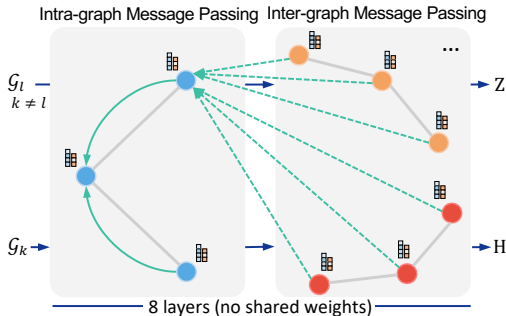


Figure 3: **IEMMN** message passing

As shown in Figure 3, we implement the encoder network Φ for representation learning by extending the design of [44]. We name it as Independent $SE(3)$ -Equivariant Multi-Graph Matching Network

(IEMMN). In specific, the Φ performs node coordinate and feature embedding updating for the input of the protein graphs $\{\mathcal{G}_k\}_{k=1}^N$, including the inter- and intra- graph message passing as well as $SE(3)$ -equivariant coordinate updates. The t -th layer of the Φ performs the update of node feature embeddings $\{\mathbf{h}_i^{(t)}\}_{i \in \cup_{k=1}^N \mathcal{V}_k}$ and node coordinate embeddings $\{\mathbf{x}_i^{(t)}\}_{i \in \cup_{k=1}^N \mathcal{V}_k}$ as:

$$\mathbf{m}_{j \rightarrow i}^{(t)} = \phi^e \left(\mathbf{h}_i^{(t)}, \mathbf{h}_j^{(t)}, \exp(-\|\mathbf{x}_i^{(t)} - \mathbf{x}_j^{(t)}\|^2 / \sigma) \mathbf{f}_{j \rightarrow i} \right), \quad \forall (i, j) \in \cup_{k=1}^N \mathcal{E}_k \quad (1)$$

$$\boldsymbol{\mu}_{j \rightarrow i}^{(t)} = a_{j \rightarrow i}^{(t)} \mathbf{W} \mathbf{h}_j^{(t)}, \quad \forall i \in \mathcal{V}_k, \quad j \in \cup_{l=1, l \neq k}^N \mathcal{V}_l \quad (2)$$

$$\mathbf{m}_i^{(t)} = \frac{1}{|\mathcal{N}(i)|} \sum_{j \in \mathcal{N}(i)} \mathbf{m}_{j \rightarrow i}^{(t)}, \quad \forall i \in \cup_{k=1}^N \mathcal{V}_k \quad (3)$$

$$\boldsymbol{\mu}_i^{(t)} = \sum_{j \in \mathcal{V}_k} \boldsymbol{\mu}_{j \rightarrow i}^{(t)}, \quad \forall i \in \mathcal{V}_k, k = 1, \dots, N \quad (4)$$

$$\mathbf{x}_i^{(t+1)} = \sum_{j \in \mathcal{N}(i)} \left(\mathbf{x}_i^{(t)} - \mathbf{x}_j^{(t)} \right) \phi^x(\mathbf{m}_{j \rightarrow i}) + \eta \mathbf{x}_i^{(0)} + (1 - \eta) \mathbf{x}_i^{(t)}, \quad \forall i \in \cup_{k=1}^N \mathcal{V}_k \quad (5)$$

$$\mathbf{h}_i^{(t+1)} = (1 - \beta) \cdot \mathbf{h}_i^{(t)} + \beta \cdot \phi^h \left(\mathbf{h}_i^{(t)}, \mathbf{m}_i^{(t)}, \boldsymbol{\mu}_i^{(t)}, \mathbf{f}_i \right), \quad \forall i \in \cup_{k=1}^N \mathcal{V}_k \quad (6)$$

where $\mathcal{N}(i)$ are the neighbors of node i ; ϕ^x is a real-valued (scalar) function; \mathbf{W} is a learnable matrix; ϕ^h, ϕ^e are functions outputting a vector \mathbb{R}^d ; $\mathbf{f}_{j \rightarrow i}$ and \mathbf{f}_i are the original edge and node features (extracted $SE(3)$ -invariantly from the residues); $a_{j \rightarrow i}$ is an attention based coefficient with trainable shallow neural networks ψ^q and ψ^k :

$$a_{j \rightarrow i}^{(t)} = \frac{\exp \left(\left\langle \psi^q \left(\mathbf{h}_i^{(t)} \right), \psi^k \left(\mathbf{h}_j^{(t)} \right) \right\rangle \right)}{\sum_{j'} \exp \left(\left\langle \psi^q \left(\mathbf{h}_i^{(t)} \right), \psi^k \left(\mathbf{h}_{j'}^{(t)} \right) \right\rangle \right)} \quad (7)$$

The output of encoder for each protein is then denoted as $\mathbf{Z} = [\mathbf{z}_1, \dots, \mathbf{z}_n] \in \mathbb{R}^{3 \times n}$, $\mathbf{H} = [\mathbf{h}_1^{(T)}, \dots, \mathbf{h}_n^{(T)}] \in \mathbb{R}^{d \times n}$, where $\mathbf{z}_i = \mathbf{x}_i^{(T)}$ for all $i \in \cup_{k=1}^N \mathcal{V}_k$. \mathbf{Z} and \mathbf{H} will be used as the input for subsequent modules. It is then straightforward to prove the following:

Proposition 4.1. $\mathbf{m}_{j \rightarrow i}, \mathbf{m}_i, \boldsymbol{\mu}_{j \rightarrow i}, \boldsymbol{\mu}_i$, and \mathbf{h}_i in the message passing of IEMMN are invariant to any orthogonal rotation $\mathbf{Q} \in \mathbb{R}^{3 \times 3}$, any translation vector $\mathbf{g} \in \mathbb{R}^3$.

Proposition 4.2. IEMMN, denoted as Φ_{IEMMN} , is rotation equivariant, i.e., for any orthogonal rotation $\mathbf{Q} \in \mathbb{R}^{3 \times 3}$, at each layer t we have: $\mathbf{Q} \mathbf{X}^{(t+1)} = \mathbf{Q} \Phi_{\text{IEMMN}}(\mathbf{X}^{(t)}) = \Phi_{\text{IEMMN}}(\mathbf{Q} \mathbf{X}^{(t)})$.

Proposition 4.3. IEMMN is translation equivariant, i.e., for any translation vector $\mathbf{g} \in \mathbb{R}^3$, at each layer t we have: $\mathbf{X}^{(t+1)} + \mathbf{g} = \Phi_{\text{IEMMN}}(\mathbf{X}^{(t)}) + \mathbf{g} = \Phi_{\text{IEMMN}}(\mathbf{X}^{(t)} + \mathbf{g})$.

Proposition 4.4. IEMMN is permutation equivariant, i.e., for any permutation operator σ on the order of \mathbf{X} , at each layer t we have: $\sigma(\mathbf{X}^{(t+1)}) = \sigma(\Phi_{\text{IEMMN}}(\mathbf{X}^{(t)})) = \Phi_{\text{IEMMN}}(\sigma(\mathbf{X}^{(t)}))$.

Therefore, the node feature embeddings \mathbf{H} is invariant by Theorem 4.1 and the node coordinate embeddings \mathbf{Z} is $SE(3)$ -equivariant and permutation equivariant by Theorems 4.2 and 4.3 and Theorem 4.4, respectively.

Estimating Pairwise Transformation and Confidence Score For each pair of proteins, the goal of pairwise protein docking is to retrieve optimal $\hat{\mathbf{R}}_{k,l}$ and $\hat{\mathbf{t}}_{k,l}$:

$$\hat{\mathbf{R}}_{k,l}, \hat{\mathbf{t}}_{k,l} = \arg \min_{\mathbf{R}_{k,l}, \mathbf{t}_{k,l}} \sum_{s=1}^{N_{\text{BP}}} \|\mathbf{R}_{k,l} \mathbf{p}_s + \mathbf{t}_{k,l} - \varphi(\mathbf{p}_s, \mathbf{q}_s)\|^2 \quad (8)$$

where N_{BP} denotes the number of binding pockets between the source and target proteins, and $\varphi(\mathbf{p}_s, \mathbf{q}_s)$ is a correspondence function that maps the pocket points $\{\mathbf{p}_s\}_{s=1}^{N_{\text{BP}}}$ to their corresponding binding points $\{\mathbf{q}_s\}_{s=1}^{N_{\text{BP}}}$ in the target protein. In our setting, the binding pockets of two interacting proteins are matched one by one, so the φ can be thought of as an identity function. In the following, we will show how to adapt the optimal transport loss and Kabsch algorithm in [44] for pairwise transformation and confidence score prediction.

Pairwise Transformation Prediction In specific, we adopt the multi-head attention mechanism to setup up M key-points queries of each protein of the input pair $\{\mathcal{G}_k, \mathcal{G}_l\}$. The set of binding keypoints predictions can be formulated as $\mathbf{y}_m^k := \sum_{i \in \mathcal{V}_k} \alpha_i^{(m)} \mathbf{z}_i^k$, for all $m \in [M]$ where $\mathbf{z}_i^k \in \mathbb{R}^3$ denotes the i -th column of the matrix \mathbf{Z}_k , and $\alpha_i^{(m)} = \text{softmax}_i \left(\frac{1}{\sqrt{d}} \mathbf{h}_i^{k\top} \mathbf{W}'_m \mu(\varphi(\mathbf{H}_l)) \right)$ are attention scores, with $\mathbf{W}'_m \in \mathbb{R}^{d \times d}$ a parametric matrix (different for each attention head), φ a linear layer plus a LeakyReLU non-linearity, and $\mu(\cdot)$ is the mean vector. We train them to approximate/superimpose the truth binding pockets of the respective protein pair. We drive such a process by assuming a *many-to-many* matching loss (i.e., optimal transport loss), which can be formulated as $\mathcal{L}_{\text{OT}} = \min_{\mathbf{T} \in \mathcal{U}(S, K)} \langle \mathbf{T}, \mathbf{C} \rangle$, where $\mathbf{C}_{m,s} = \|\mathbf{y}_{km} - \mathbf{p}_{ks}\|^2 + \|\mathbf{y}_{lm} - \mathbf{p}_{ls}\|^2$, and $\mathcal{U}(S, M)$ is the set of $S \times M$ transport plans with uniform marginals \mathbf{p}_k is the binding points of protein k . Next, given the pocket point prediction $\mathbf{Y}_k, \mathbf{Y}_l$, the relative transformation $\mathbf{R}_{k,l}$ from the source protein to the target protein can easily be calculated by a differentiable ordered point sets registration algorithm (e.g., Kabsch algorithm) as: $\mathbf{R}_{k,l}, \mathbf{t}_{k,l} = \mathcal{F}_{\text{reg}}(\mathbf{Y}_k, \mathbf{Y}_l)$

Pairwise Confidence Estimation. Synchronization is more effective when weights are provided for each of the pairwise estimates. We weight each pairwise transformation, formulate the estimation of $c_{k,l}$ as a binary classification task, and define the confidence estimation function as

$$c_{k,l} \leftarrow \Phi_{\text{con}}(\mathbf{x}_k \otimes \mathbf{T}_{k,l}, \mathbf{x}_j, \mathbf{h}_k, \mathbf{h}_l) \quad (9)$$

where the input consists of (i) the coordinates of the transformed source and target proteins, the \otimes is the affine transformation function that aligns the source and target proteins, (ii) the feature/latent vector of proteins. We use a mean operator to generate features. These features are combined and fed into a confidence estimation network with three fully connected layers (64-64-32-1) and a sigmoid activation function. The output of this network is a score $c_{k,l}$ which is a value between 0 and 1. The corresponding ground truth $c_{k,l}^{\text{GT}}$ is obtained directly from the training data. To avoid redundant computations, we only estimate pairwise pose predictions and scores for pairs (k, l) where $k < l$. For pairs $k > l$, we set $c_{l,k} = c_{k,l}$, $\mathbf{R}_{l,k} = \mathbf{R}_{k,l}^{-1}$, and $\mathbf{t}_{l,k} = \mathbf{R}_{k,l} \cdot \mathbf{t}_{k,l}$. The training of the pairwise protein docking module is directly supervised by the combination of the relative transformation loss \mathcal{L}_{REL} and the confidence loss function \mathcal{L}_{CON} , where the \mathcal{L}_{CON} denotes the binary cross entropy loss, and

$$\mathcal{L}_{\text{REL}} = \sum_{(k,l) \in \mathcal{S}} \left(\|\mathbf{R}_{k,l} - \mathbf{R}_{k,l}^{\text{GT}}\|_2 + \|\mathbf{t}_{k,l} - \mathbf{t}_{k,l}^{\text{GT}}\|_2 \right). \quad (10)$$

SE(3) Transformation Synchronization Given the estimated $\binom{N}{2}$ relative protein-to-protein transformations, we aim to find the N global absolute transformations $\{\mathbf{T}_k\}$ that best explain them. Previous method [46, 47] proposed a closed-form solution to $SE(3)$ synchronization using spectral decomposition. This idea was further developed in end-to-end learning pipelines [48, 49]. The approach is based on the construction of a block matrix of pairwise transformations, where the block (k, l) represents the transformation between instance k and l . The key insight in this line of research is that the absolute transformations can be extracted from the pairwise transformation matrix by means of eigendecomposition. The global transformation parameters can be determined either through joint calculation (also known as transformation synchronization) or by breaking the problem into two parts: rotation synchronization and translation synchronization. In this paper, we opt for the latter approach, dividing the problem into rotational and translational synchronization, which admits a differentiable closed-form solution under the spectral relation.

Rotation Synchronization. Our approach to rotation synchronization is based on a Laplacian rotation synchronization formulation that has been proposed previously in the literature [48]: $\mathbf{R}_k^* = \arg \min_{\mathbf{R}_k \in SO(3)} \sum_{(k,l) \in \mathcal{E}} c_{k,l} \|\mathbf{R}_{k,l} - \mathbf{R}_k \mathbf{R}_l^\top\|_F^2$. More precisely, consider a symmetric matrix $\mathbf{L} \in \mathbb{R}^{3N \times 3N}$, which resembles a block Laplacian matrix, defined as:

$$\mathbf{L} = \begin{bmatrix} \mathbf{I}_3 \sum_i c_{k,1} & -c_{1,2} \mathbf{R}_{1,2} & \cdots & -c_{1,N} \mathbf{R}_{1,N} \\ -c_{2,1} \mathbf{R}_{2,1} & \mathbf{I}_3 \sum_i c_{k,2} & \cdots & -c_{2,N} \mathbf{R}_{2,N} \\ \vdots & \vdots & \ddots & \vdots \\ -c_{N,1} \mathbf{R}_{N,1} & -c_{N,2} \mathbf{R}_{N,2} & \cdots & \mathbf{I}_3 \sum_i c_{k,N} \end{bmatrix}.$$

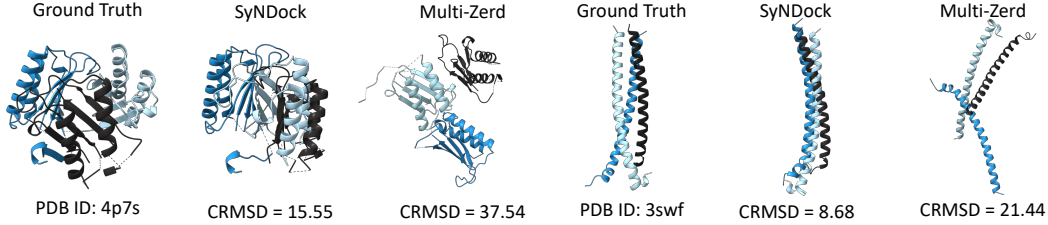


Figure 4: **Complex Prediction Visualization.** Qualitative comparisons between our approach and baseline approaches on the trimeric protein samples.

where the $c_{k,l}$ represents the pairwise confidence score. $\mathbf{R}_{k,l}$ is the estimated relative rotation transformation, and the N is denoted as the number of input protein chains. Consequently, we collect the three eigenvectors $\mathbf{U} = (\mathbf{U}_1^\top, \dots, \mathbf{U}_N^\top)^\top \in \mathbb{R}^{3N \times 3}$ that correspond to the three smallest eigenvalues of \mathbf{L} . To avoid reflections, we choose the sign of each eigenvector such that $\sum_{i=1}^N \det(\mathbf{U}_k) > 0$. The least squares estimates of the global rotation matrices \mathbf{R}_i are then given, under relaxed orthogonality and determinant constraints, by first performing singular value decomposition (SVD) on each $\mathbf{U}_k = \mathbf{V}_k \mathbf{\Sigma}_k \mathbf{W}_k^\top$ and then output the corresponding absolute rotation estimate as:

$$\mathbf{R}_k = \mathbf{V}_k \mathbf{W}_k^\top, \quad \text{for all } k = 1, 2, \dots, N. \quad (11)$$

Translation Synchronization. We can retrieve global translation vectors $\{\mathbf{t}_k\}$ that minimize the following least squares problem:

$$\mathbf{t}_k = \arg \min_{\mathbf{t}_k} \sum_{(k,l) \in \mathcal{E}} c_{k,l} \left\| \hat{\mathbf{R}}_{k,l} \mathbf{t}_k + \hat{\mathbf{t}}_{k,l} - \mathbf{t}_l \right\|^2 \quad (12)$$

The closed-form solution is easy to get: $\mathbf{t} = \mathbf{L}^+ \mathbf{b}$, where $\mathbf{t}^* = [\mathbf{t}_1^{*\top}, \dots, \mathbf{t}_N^{*\top}]^\top \in \mathbb{R}^{3N}$ and $\mathbf{b} = [\mathbf{b}_1^{*\top}, \dots, \mathbf{b}_N^{*\top}]^\top \in \mathbb{R}^{3N}$ with $\mathbf{b}_k := -\sum_{l \in \mathcal{N}(k)} c_{k,l} \mathbf{R}_{k,l}^\top \mathbf{t}_{k,l}$.

Iterative Refinement of N -body Docking. The above formulation allows an implementation in an iterative scheme, with the ability to refine the predictions step by step, starting from a coarse level. To this end, we can start each subsequent iteration by using the synchronized estimated parameters \mathbf{T}_k from the previous iteration to fit each protein, setting $\mathbf{X}_k^* = \mathbf{X}_k \otimes \mathbf{T}_k$. In this paper, we iterate the refinement 4 times for each sample and calculate the loss with the final prediction.

End-to-End Training Algorithm We supervise the network training using the following supervisions: \mathcal{L}_{REL} , \mathcal{L}_{CON} , \mathcal{L}_{OT} as well as the global *Synchronization Loss*: $\mathcal{L}_{\text{SYNC}} = \frac{1}{N} \sum_{k=1}^N \|\mathbf{X}_k \otimes \mathbf{T}_k - \mathbf{X}_k^{\text{GT}}\|_2$ where \otimes is the affine transformation. The total loss functions can thus be defined as

$$\mathcal{L}_{\text{OVERALL}} = \mathcal{L}_{\text{OT}} + \mathcal{L}_{\text{REL}} + \mathcal{L}_{\text{CON}} + \mathcal{L}_{\text{SYNC}}. \quad (13)$$

5 Experiments

Dataset. We evaluated our method on the DIPS dataset [51], which is currently the largest protein complex structure dataset mined from the Protein Data Bank and tailored to the rigid body docking assumption. We adopted the same split as defined in EquiDock [44], where the train/validation/test splits are based on the protein family. After excluding a few structures with more than 10K atoms, we get 14,225 PDB for the training set, 368 for the validation set, and 393 for the test. To generate subsets of N -body protein complexes, we extracted connected subgraphs with N degrees and removed complexes with more than ten chains. The statistics of the curated dataset is in Table 1. We also performed a binary docking evaluation in Table 3, using the default settings provided by [44], which included 100 randomly

Table 1: **Curated dataset statistics.**

N-Body	Train	Valid	Test
2	30,299	748	887
3	19,664	441	593
4	16,415	303	429
5	14,105	251	257
6	10,689	281	114
7	5,881	220	30
8	2,143	90	5
9	545	20	0
10	53	2	0

Table 2: **Multimeric Complex Prediction Result.** Comparison between Multi Zerd [52] and SyNDock in two performance metrics in the two curated subsets (N=3,4). All values are smaller the better. We can see that SyNDock can significantly outperform Multi-Zerd in terms of docking accuracy as well as having a clear advantage in the identification of docking sites.

Methods	Trimer (N=3)						Tetramer (N=4)					
	Complex-RMSD ↓			Interface-RMSD ↓			Complex-RMSD ↓			Interface-RMSD ↓		
	Median	Mean	Std	Median	Mean	Std	Median	Mean	Std	Median	Mean	Std
Multi-Zerd	22.17	24.06	6.08	23.16	24.44	6.95	28.51	29.02	5.83	26.75	29.23	8.71
SyNDock	21.02	22.01	7.69	17.80	18.35	6.34	23.92	24.56	7.12	19.75	20.37	5.85

selected test pairs from the DIPS dataset. We refer the readers to Appendix B for more detailed information on the mentioned datasets as well as curation implementation.

Evaluation Metrics. We use two metrics to measure the quality of the docking predictions: Complex Root Mean Square Deviation (C-RMSD) and Interface Root Mean Square Deviation (I-RMSD). These two metrics are defined below: Given the ground truth $\mathbf{P}^* \in \mathbb{R}^{3 \times \sum_{k=1}^N n_k}$ and predicted complex structures $\mathbf{P} \in \mathbb{R}^{3 \times \sum_{k=1}^N n_k}$, we first superimpose them using the rigid registration algorithm (i.e., Kabsch) and then compute the C-RMSD as $\sqrt{\frac{1}{\sum_{k=1}^N n_k} \|\mathbf{P}^* - \mathbf{P}\|_F^2}$. The I-RMSD is calculated similarly, but only takes the coordinates of the residues that are within 8 angstroms of the residues in the other protein. For a fair comparison between the baselines, we use only the α carbon coordinates for the calculation of both metrics.

Experimental Configurations. We train our model using the AdamW optimizer with a learning rate of 10^{-4} and a weight decay of 10^{-3} . We train for 50 epochs with a batch size of 6 using a fixed learning rate schedule. Model selection is based on the performance of the validation set. The best validation model is then tested on the test set. Unless otherwise noted, we train and test separately on different N-body data subsets. For data augmentation, we randomly change the permutation of inputs during training and testing, and we also randomly rotate and translate all inputs in the space. Our implementation is based on the PyTorch toolkit [53], with extensive use of the ROMA [52] package. We will make our code available to the public.

Multimeric Protein Docking. We compare SyNDock to the widely used multimeric protein docking method Multi-Zerd [13]. Note that there are very few open-source, user-friendly multimeric docking programs available for comparison, and some of them (CombDock² [16], RL-Multi-LzerD³ [14]) always crash. For different subsets of N bodies, we randomly select a certain number of test samples from the test set for comparison (60 samples for trimer, 30 samples for tetramer). From Table 2 we see that SyNDock significantly outperforms Multi-Zerd, especially in the tetramer docking subset ($N = 4$), where the former increases the C-RMSD by up to 4.5% compared to the latter. This observation holds true for the I-RMSD metrics as well, demonstrating that our method also has a clear advantage in binding site identification. Furthermore, our method exhibits a speed improvement of several orders of magnitude compared to the baseline method (see Figure 5).

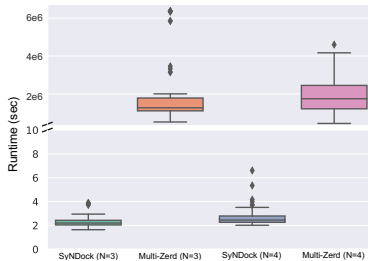
Binary Protein Docking. SyNDock can be scaled down to predict binary protein docking. We compare SyNDock to the popular binary protein docking baselines: Attract [7], HDock [41], ClusPro [9], PatchDock [54], and the recently proposed EquiDock [44]. As shown in Table 3, SyNDock is competitive and often outperforms the baselines, demonstrating that our method also has a general capability.

²<http://bioinfo3d.cs.tau.ac.il/CombDock/download/>

³<https://github.com/kiharalab/RL-MLZerd>

Table 3: **Binary Complex Prediction Results.** Comparison of different binary docking methods. Figure 5: **Inference time distribution.** Both methods are tested on the same hardware.

Methods	Complex-RMSD			Interface-RMSD		
	Median	Mean	Std	Median	Mean	Std
Attract	17.17	14.93	10.39	12.41	14.02	11.81
HDock	6.23	10.77	11.39	3.90	8.88	10.95
ClusPro	15.76	14.47	10.24	12.54	13.62	11.11
PatchDock	15.24	13.58	10.30	11.44	12.15	10.50
EquiDock	13.29	14.52	7.13	10.18	11.92	7.01
SyNDock	12.95	14.27	6.85	9.97	11.93	5.84



Computation Efficiency. Figure 5 compares the inference efficiency of different approaches. We record the running time of all complex structure prediction algorithms on the trimer and tetramer test set. Note that SyNDock predicts the global transformation in a direct shot, resulting in speeds several orders of magnitude faster than the baseline method. This is particularly advantageous for intensive screening applications that need to search over large search spaces, such as drug discovery. In addition, as the number of input proteins increases, the superiority of SyNDock in terms of speed becomes increasingly apparent.

Ablation Study. We conduct an ablation study on the trimer test set to assess the significance of the core modules in SyNDock. As a baseline, we implement a heuristic method called *EquiDock-Seq*, which sequentially docks proteins using a binary docking model (*EquiDock*). As shown in Table 4, *EquiDock-Seq* fails to effectively address the challenges of multiple protein docking, resulting in C-RMSD and I-RMSD scores of 25.7 and 26.2, respectively. To evaluate the impact of the learnable synchronization module, we introduce the synchronization module to the pipeline, enabling a learning-centric solution (*SyNDock wo IEMNN*). This integration significantly improves the performance, achieving C-RMSD and I-RMSD scores of 22.9 and 19.8, respectively. Next, we investigate the effectiveness of the proposed IEMNN backbone by replacing the backbone of the previous experiments. For the baseline approach (*SyNDock wo sync*), we observe a slight improvement in I-RMSD to 20.4, while C-RMSD remains unchanged. The best performance is achieved by *SyNDock* (standard) with C-RMSD and I-RMSD scores of 22.0 and 18.4, respectively, demonstrates the effectiveness of the IEMNN backbone in aggregating and propagating information across multiple graphs. Overall, the ablation study highlights the importance and effectiveness of the proposed modules in improving the multimeric protein docking performance.

Table 4: **Ablation study** (Trimer test set)

Method	IEMNN	SyNc	C-RMSD	I-RMSD
<i>EquiDock-Seq</i>	×	×	25.7	26.2
<i>SyNDock</i>	✓	×	25.5	20.4
<i>SyNDock</i>	×	✓	22.9	19.8
<i>SyNDock</i>	✓	✓	22.0	18.4

Visualization In Figure 4, we show a number of successful examples where *SyNDock* has significantly outperformed the baselines on the subset of trimeric proteins.

6 Conclusions

In this paper, we propose a novel multimeric protein docking model, *SyNDock*, which allows effective learning to assemble the complex in a globally consistent manner, opening a new perspective on multimeric complex docking. It enables the automatic assembly of accurate multimeric complexes within a few seconds, the performance of which can be superior or comparable to recent advanced approaches. Extensive experiments on our curated dataset show that *SyNDock* outperforms advanced methods in both accuracy and speed. Regarding limitations, we acknowledge two main aspects. Firstly, limited by the rare number of resolved multibody protein structures, we expanded the number by extracting substructures. However, this may introduce biases and deviate from the true distribution of protein complexes in nature. This limitation is inherent to the data generation process and can potentially impact the performance and generalizability of the trained models. Secondly, our approach relies on the rigid assumption, which restricts its applicability to flexible protein docking scenarios. For future work, we would like to incorporate more domain knowledge and extend the current framework to more applications.

References

- [1] James D Watson and Francis HC Crick. Molecular structure of nucleic acids: a structure for deoxyribose nucleic acid. *Nature*, 171(4356):737–738, 1953.
- [2] Marshall W Nirenberg and J Heinrich Matthaei. The dependence of cell-free protein synthesis in *e. coli* upon naturally occurring or synthetic polyribonucleotides. *Proceedings of the National Academy of Sciences*, 47(10):1588–1602, 1961.
- [3] Mark A Lemmon and Joseph Schlessinger. Cell signaling by receptor tyrosine kinases. *Cell*, 141(7):1117–1134, 2010.
- [4] William Henry Bragg and William Lawrence Bragg. The reflection of x-rays by crystals. *Proceedings of the Royal Society of London. Series A, Containing Papers of a Mathematical and Physical Character*, 88(605):428–438, 1913.
- [5] Charles Christoffer, Siyang Chen, Vijay Bharadwaj, Tunde Aderinwale, Vidhur Kumar, Matin Hormati, and Daisuke Kihara. Lzerd webserver for pairwise and multiple protein–protein docking. *Nucleic Acids Research*, 49(W1):W359–W365, 2021.
- [6] Cyril Dominguez, Rolf Boelens, and Alexandre MJJ Bonvin. Haddock: a protein- protein docking approach based on biochemical or biophysical information. *Journal of the American Chemical Society*, 125(7):1731–1737, 2003.
- [7] Sjoerd de Vries and Martin Zacharias. Flexible docking and refinement with a coarse-grained protein model using attract. *Proteins: Structure, Function, and Bioinformatics*, 81(12):2167–2174, 2013.
- [8] Julian Mintseris, Brian Pierce, Kevin Wiehe, Robert Anderson, Rong Chen, and Zhiping Weng. Integrating statistical pair potentials into protein complex prediction. *Proteins: Structure, Function, and Bioinformatics*, 69(3):511–520, 2007.
- [9] Dima Kozakov, David R Hall, Bing Xia, Kathryn A Porter, Dzmitry Padhorny, Christine Yueh, Dmitri Beglov, and Sandor Vajda. The cluspro web server for protein–protein docking. *Nature protocols*, 12(2):255–278, 2017.
- [10] Sergey Lyskov and Jeffrey J Gray. The rosettdock server for local protein–protein docking. *Nucleic acids research*, 36(suppl_2):W233–W238, 2008.
- [11] Mieczyslaw Torchala, Iain H Moal, Raphael AG Chaleil, Juan Fernandez-Recio, and Paul A Bates. Swarmdock: a server for flexible protein–protein docking. *Bioinformatics*, 29(6):807–809, 2013.
- [12] David W Ritchie and Vishwesh Venkatraman. Ultra-fast fft protein docking on graphics processors. *Bioinformatics*, 26(19):2398–2405, 2010.
- [13] Juan Esquivel-Rodríguez, Yifeng David Yang, and Daisuke Kihara. Multi-lzerd: multiple protein docking for asymmetric complexes. *Proteins: Structure, Function, and Bioinformatics*, 80(7):1818–1833, 2012.
- [14] Tunde Aderinwale, Charles Christoffer, and Daisuke Kihara. Rl-mlzerd: Multimeric protein docking using reinforcement learning. *Frontiers in Molecular Biosciences*, 9, 2022.
- [15] David W Ritchie and Sergei Grudinin. Spherical polar fourier assembly of protein complexes with arbitrary point group symmetry. *Journal of Applied Crystallography*, 49(1):158–167, 2016.
- [16] Yuval Inbar, Hadar Benyamini, Ruth Nussinov, and Haim J Wolfson. Prediction of multimolecular assemblies by multiple docking. *Journal of molecular biology*, 349(2):435–447, 2005.
- [17] Juan Esquivel-Rodríguez, Yifeng David Yang, and Daisuke Kihara. Multi-lzerd: multiple protein docking for asymmetric complexes. *Proteins: Structure, Function, and Bioinformatics*, 80(7):1818–1833, 2012.
- [18] Raphael Townshend, Rishi Bedi, Patricia Suriana, and Ron Dror. End-to-end learning on 3d protein structure for interface prediction. *Advances in Neural Information Processing Systems*, 32, 2019.
- [19] John Jumper, Richard Evans, Alexander Pritzel, Tim Green, Michael Figurnov, Olaf Ronneberger, Kathryn Tunyasuvunakool, Russ Bates, Augustin Židek, Anna Potapenko, et al. Highly accurate protein structure prediction with alphafold. *Nature*, 596(7873):583–589, 2021.

- [20] Minkyung Baek, Frank DiMaio, Ivan Anishchenko, Justas Dauparas, Sergey Ovchinnikov, Gyu Rie Lee, Jue Wang, Qian Cong, Lisa N Kinch, R Dustin Schaeffer, et al. Accurate prediction of protein structures and interactions using a three-track neural network. *Science*, 373(6557):871–876, 2021.
- [21] Method of the year 2021: Protein structure prediction. *Nature Methods*, 19(1):1–1, Jan 2022.
- [22] Junsu Ko and Juyong Lee. Can alphafold2 predict protein-peptide complex structures accurately? *BioRxiv*, 2021.
- [23] Tomer Tsaban, Julia K Varga, Orly Avraham, Ziv Ben-Aharon, Alisa Khramushin, and Ora Schueler-Furman. Harnessing protein folding neural networks for peptide–protein docking. *Nature communications*, 13(1):1–12, 2022.
- [24] Patrick Bryant, Gabriele Pozzati, and Arne Elofsson. Improved prediction of protein–protein interactions using alphafold2. *Nature communications*, 13(1):1–11, 2022.
- [25] Laurent Maveyraud and Lionel Mourey. Protein x-ray crystallography and drug discovery. *Molecules*, 25(5):1030, 2020.
- [26] Zbigniew Dauter and Alexander Wlodawer. Progress in protein crystallography. *Protein and peptide letters*, 23(3):201–210, 2016.
- [27] Gottfried Otting. Protein nmr using paramagnetic ions. *Annual review of biophysics*, 39:387–405, 2010.
- [28] Christoph Nitsche, Gottfried Otting, et al. Pseudocontact shifts in biomolecular nmr using paramagnetic metal tags. 2017.
- [29] Jonas Pfab, Nhut Minh Phan, and Dong Si. Deepracer for fast de novo cryo-em protein structure modeling and special studies on cov-related complexes. *Proceedings of the National Academy of Sciences*, 118(2):e2017525118, 2021.
- [30] Tiago RD Costa, Athanasios Ignatiou, and Elena V Orlova. Structural analysis of protein complexes by cryo electron microscopy. *Bacterial protein secretion systems*, pages 377–413, 2017.
- [31] Chi-Min Ho, Xiaorun Li, Mason Lai, Thomas C Terwilliger, Josh R Beck, James Wohlschlegel, Daniel E Goldberg, Anthony WP Fitzpatrick, and Z Hong Zhou. Bottom-up structural proteomics: cryoem of protein complexes enriched from the cellular milieu. *Nature methods*, 17(1):79–85, 2020.
- [32] Ilya A Vakser. Protein-protein docking: From interaction to interactome. *Biophysical journal*, 107(8):1785–1793, 2014.
- [33] Sjoerd J De Vries, Marc Van Dijk, and Alexandre MJJ Bonvin. The haddock web server for data-driven biomolecular docking. *Nature protocols*, 5(5):883–897, 2010.
- [34] Rong Chen, Li Li, and Zhiping Weng. Zdock: an initial-stage protein-docking algorithm. *Proteins: Structure, Function, and Bioinformatics*, 52(1):80–87, 2003.
- [35] Jacek Biesiada, Aleksey Porollo, Prakash Velayutham, Michal Kouril, and Jaroslaw Meller. Survey of public domain software for docking simulations and virtual screening. *Human genomics*, 5(5):1–9, 2011.
- [36] Christina EM Schindler, Isaure Chauvot de Beauchêne, Sjoerd J de Vries, and Martin Zacharias. Protein-protein and peptide-protein docking and refinement using attract in capri. *Proteins: Structure, Function, and Bioinformatics*, 85(3):391–398, 2017.
- [37] Gaoqi Weng, Ercheng Wang, Zhe Wang, Hui Liu, Feng Zhu, Dan Li, and Tingjun Hou. Hawkdock: a web server to predict and analyze the protein–protein complex based on computational docking and mm/gbsa. *Nucleic acids research*, 47(W1):W322–W330, 2019.
- [38] Sharon Sunny and PB Jayaraj. Fpdock: Protein–protein docking using flower pollination algorithm. *Computational Biology and Chemistry*, 93:107518, 2021.
- [39] Charles Christoffer, Siyang Chen, Vijay Bharadwaj, Tunde Aderinwale, Vidhur Kumar, Matin Hormati, and Daisuke Kihara. Lzard webserver for pairwise and multiple protein–protein docking. *Nucleic Acids Research*, 2021.
- [40] Vishwesh Venkatraman, Yifeng D Yang, Lee Sael, and Daisuke Kihara. Protein-protein docking using region-based 3d zernike descriptors. *BMC bioinformatics*, 10(1):1–21, 2009.

- [41] Yumeng Yan, Huanyu Tao, Jiahua He, and Sheng-You Huang. The hdock server for integrated protein–protein docking. *Nature protocols*, 15(5):1829–1852, 2020.
- [42] Mieczyslaw Torchala, Iain H Moal, Raphael AG Chaleil, Juan Fernandez-Recio, and Paul A Bates. Swarmdock: a server for flexible protein–protein docking. *Bioinformatics*, 29(6):807–809, 2013.
- [43] Jacob Verburgt and Daisuke Kihara. Benchmarking of structure refinement methods for protein complex models. *Proteins: Structure, Function, and Bioinformatics*, 2021.
- [44] Octavian-Eugen Ganea, Xinyuan Huang, Charlotte Bunne, Yatao Bian, Regina Barzilay, Tommi S. Jaakkola, and Andreas Krause. Independent SE(3)-equivariant models for end-to-end rigid protein docking. In *International Conference on Learning Representations*, 2022.
- [45] Yuval Inbar, Hadar Benyamini, Ruth Nussinov, and Haim J Wolfson. Protein structure prediction via combinatorial assembly of sub-structural units. *Bioinformatics*, 19(suppl_1):i158–i168, 2003.
- [46] Federica Arrigoni, Beatrice Rossi, and Andrea Fusiello. Spectral synchronization of multiple views in se (3). *SIAM Journal on Imaging Sciences*, 9(4):1963–1990, 2016.
- [47] Federica Arrigoni, Luca Magri, Beatrice Rossi, Pasqualina Fragneto, and Andrea Fusiello. Robust absolute rotation estimation via low-rank and sparse matrix decomposition. In *2014 2nd International Conference on 3D Vision*, volume 1, pages 491–498. IEEE, 2014.
- [48] Zan Gojcic, Caifa Zhou, Jan D Wegner, Leonidas J Guibas, and Tolga Birdal. Learning multiview 3d point cloud registration. In *Proceedings of the IEEE/CVF conference on computer vision and pattern recognition*, pages 1759–1769, 2020.
- [49] Xiangru Huang, Zhenxiao Liang, Xiaowei Zhou, Yao Xie, Leonidas J Guibas, and Qixing Huang. Learning transformation synchronization. In *Proceedings of the IEEE/CVF Conference on Computer Vision and Pattern Recognition*, pages 8082–8091, 2019.
- [50] Bowen Jing, Stephan Eismann, Patricia Suriana, Raphael JL Townshend, and Ron Dror. Learning from protein structure with geometric vector perceptrons. *arXiv preprint arXiv:2009.01411*, 2020.
- [51] Raphael Townshend, Rishi Bedi, Patricia Suriana, and Ron Dror. End-to-end learning on 3d protein structure for interface prediction. *Advances in Neural Information Processing Systems*, 32, 2019.
- [52] Romain Brégier. Deep regression on manifolds: a 3d rotation case study. In *2021 International Conference on 3D Vision (3DV)*, pages 166–174. IEEE, 2021.
- [53] Adam Paszke, Sam Gross, Soumith Chintala, Gregory Chanan, Edward Yang, Zachary DeVito, Zeming Lin, Alban Desmaison, Luca Antiga, and Adam Lerer. Automatic differentiation in pytorch. 2017.
- [54] Efrat Mashiach, Dina Schneidman-Duhovny, Aviyah Peri, Yoli Shavit, Ruth Nussinov, and Haim J Wolfson. An integrated suite of fast docking algorithms. *Proteins: Structure, Function, and Bioinformatics*, 78(15):3197–3204, 2010.

Appendix

Contents

A	Notations and Proofs	13
A.1	Notations	13
A.2	Proofs	13
B	Implementations	14
B.1	Algorithm	14
B.2	Dataset	15
B.3	Data representation	15

A Notations and Proofs

A.1 Notations

We compile a comprehensive list of all the notations utilized in this paper, as shown in Table 5.

Table 5: Notations.

Notation	Description
$\mathbf{R}_{k,l} \in SO(3)$	the relative rotation matrix between protein k and l
$\mathbf{R}_k \in SO(3)$	the absolute rotation matrix of protein k
$\mathbf{t}_k \in \mathbb{R}^3$	the translation vector of protein k
$\mathbf{T}_k \in SE(3) \subset \mathbb{R}^{4 \times 4}$	the transformation matrix of protein k
\mathcal{V}_k	a set of n_k nodes where each node $v \in \mathcal{V}_k$ represents an amino acid in protein k
$\mathcal{N}(i)$	the set of neighborhood nodes of node i
\mathcal{E}_k	a set of edges where each edge $e_{i,j} \in \mathcal{E}_k$ exists if amino acid $j \in \mathcal{N}(i)$ in protein k
$\mathbf{X}_k \in \mathbb{R}^{3 \times n_k}$	the Cartesian coordinate matrix of the α -carbon atoms of a protein k
$\mathbf{x}_i \in \mathbb{R}^3$	the Cartesian coordinate vector of a α -carbon atom where \mathbf{x}_i is the i -th column of a \mathbf{X}
$\mathbf{h}_i \in \mathbb{R}^{f_1}$	the f_1 -dimensional feature vector of a node (amino acid)
$\mathbf{f}_i \in \mathbb{R}^{f_2}$	the additional f_2 -dimensional feature vector of a node
$\mathbf{f}_{j \rightarrow i} \in \mathbb{R}^{f_3}$	the additional f_3 -dimensional feature vector of an edge between node i and j
$\mathcal{G} = (\mathcal{V}, \mathcal{E})$	a protein graphs where each node represents each amino acid in the protein
$\mathcal{S} = \{\mathcal{G}_i, 1 \leq i \leq N\}$	a set of proteins where each graph $\mathcal{G}_i = (\mathcal{V}_i, \mathcal{E}_i)$
$\mathbf{p}_{k,l} \in \mathbb{R}^{3 \times m}$	pocket points between proteins k and l
$c_{k,l}$	the estimated confidence between protein k and l
$\mathbf{Z}_k = \mathbf{X}_k^{(T)} \in \mathbb{R}^{3 \times n_k}$	the output coordinate node embeddings of IEMMN for protein k
$\mathbf{H}_k \in \mathbb{R}^{d \times n_k}$	the node embeddings of protein k
u	the number of total iterations

A.2 Proofs

In this part, we present the proof of the theorem proposed in the main paper.

A.2.1 Proof of Theorem 4.1

Proof. Assume that $\mathbf{h}^{(0)}$ is invariant to any orthogonal rotation and translation. By Equations (2) and (4), $\boldsymbol{\mu}_{j \rightarrow i}, \boldsymbol{\mu}$ are obviously invariant.

Note that for any orthogonal rotation $\mathbf{Q} \in \mathbb{R}^{3 \times 3}$,

$$\begin{aligned} \|\mathbf{Q}\mathbf{x}_i^{(t)} - \mathbf{Q}\mathbf{x}_j^{(t)}\| &= (\mathbf{x}_i^{(t)} - \mathbf{x}_j^{(t)})^\top \mathbf{Q}^\top \mathbf{Q} (\mathbf{x}_i^{(t)} - \mathbf{x}_j^{(t)}) \\ &= (\mathbf{x}_i^{(t)} - \mathbf{x}_j^{(t)})^\top \mathbf{I} (\mathbf{x}_i^{(t)} - \mathbf{x}_j^{(t)}) \end{aligned}$$

$$= \|\mathbf{x}_i^{(t)} - \mathbf{x}_j^{(t)}\|^2,$$

and any translation $\mathbf{g} \in \mathbb{R}^3$,

$$\|\mathbf{x}_i^{(t)} + \mathbf{g} - (\mathbf{x}_j^{(t)} + \mathbf{g})\| = \|\mathbf{x}_i^{(t)} - \mathbf{x}_j^{(t)}\|,$$

Then by Equations (1) and (3), we also have $\mathbf{m}_{j \rightarrow i}$, \mathbf{m}_i are also invariant. Therefore, by Equation (6) we obtain $\mathbf{h}_i^{(t+1)}$ is also invariant, which complete the proof. \square

A.2.2 Proof of Theorem 4.2

Proof. By Theorem 4.1, we know that \mathbf{m}_i is invariant to any orthogonal rotation. Then, for any orthogonal rotation $\mathbf{Q} \in \mathbb{R}^{3 \times 3}$,

$$\begin{aligned} & \eta \mathbf{Q} \mathbf{x}_i^{(0)} + (1 - \eta) \mathbf{Q} \mathbf{x}_i^{(t)} + \sum_{j \in \mathcal{N}(i)} \left(\mathbf{Q} \mathbf{x}_i^{(t)} - \mathbf{Q} \mathbf{x}_j^{(t)} \right) \phi^x(\mathbf{m}_{j \rightarrow i}) \\ &= \eta \mathbf{Q} \mathbf{x}_i^{(0)} + (1 - \eta) \mathbf{Q} \mathbf{x}_i^{(t)} + \sum_{j \in \mathcal{N}(i)} \mathbf{Q} \left(\mathbf{x}_i^{(t)} - \mathbf{x}_j^{(t)} \right) \phi^x(\mathbf{m}_{j \rightarrow i}) \\ &= \eta \mathbf{Q} \mathbf{x}_i^{(0)} + (1 - \eta) \mathbf{Q} \mathbf{x}_i^{(t)} + \mathbf{Q} \left(\sum_{j \in \mathcal{N}(i)} \left(\mathbf{x}_i^{(t)} - \mathbf{x}_j^{(t)} \right) \phi^x(\mathbf{m}_{j \rightarrow i}) \right) \\ &= \mathbf{Q} \left(\eta \mathbf{x}_i^{(0)} + (1 - \eta) \mathbf{x}_i^{(t)} + \sum_{j \in \mathcal{N}(i)} \left(\mathbf{x}_i^{(t)} - \mathbf{x}_j^{(t)} \right) \phi^x(\mathbf{m}_{j \rightarrow i}) \right) \\ &= \mathbf{Q} \mathbf{x}_i^{(t+1)}. \end{aligned}$$

\square

A.2.3 Proof of Theorem 4.3

Proof. By Theorem 4.1, we know that \mathbf{m}_i is invariant to any translation. Then, for any translation $\mathbf{g} \in \mathbb{R}^3$,

$$\begin{aligned} & \eta (\mathbf{x}_i^{(0)} + \mathbf{g}) + (1 - \eta) (\mathbf{x}_i^{(t)} + \mathbf{g}) + \sum_{j \in \mathcal{N}(i)} \left((\mathbf{x}_i^{(t)} + \mathbf{g}) - (\mathbf{x}_j^{(t)} + \mathbf{g}) \right) \phi^x(\mathbf{m}_{j \rightarrow i}) \\ &= \eta \mathbf{x}_i^{(0)} + \eta \mathbf{g} + (1 - \eta) \mathbf{x}_i^{(t)} + (1 - \eta) \mathbf{g} + \sum_{j \in \mathcal{N}(i)} \left(\mathbf{x}_i^{(t)} - \mathbf{x}_j^{(t)} \right) \phi^x(\mathbf{m}_{j \rightarrow i}) \\ &= \eta \mathbf{x}_i^{(0)} + (1 - \eta) \mathbf{x}_i^{(t)} + \sum_{j \in \mathcal{N}(i)} \left(\mathbf{x}_i^{(t)} - \mathbf{x}_j^{(t)} \right) \phi^x(\mathbf{m}_{j \rightarrow i}) + \mathbf{g} \\ &= \mathbf{x}_i^{(t+1)} + \mathbf{g}. \end{aligned}$$

\square

A.2.4 Proof of Theorem 4.4

Proof. For any permutation σ on the order of \mathbf{X} , denoted by $\sigma(i)$ as the permuted index for i . Obviously we have,

$$\eta \mathbf{x}_{\sigma(i)}^{(0)} + (1 - \eta) \mathbf{x}_{\sigma(i)}^{(t)} + \sum_{j \in \mathcal{N}(\sigma(i))} \left(\mathbf{x}_{\sigma(i)}^{(t)} - \mathbf{x}_j^{(t)} \right) \phi^x(\mathbf{m}_{j \rightarrow \sigma(i)}) = \mathbf{x}_{\sigma(i)}^{(t+1)}$$

\square

B Implementations

B.1 Algorithm

As a supplement to method described in the main paper, we provide the implementation details in Algorithm 1 for better clarity.

Algorithm 1: SyNDock

Input: $\mathcal{G}_k = (\mathcal{V}_k, \mathcal{E}_k)$ **Output:** $T^*(\mathbf{R}_k, \mathbf{t}_k)$ **Function** SYNCDOCK(F):

Extract multi-graph features using the IEMMN backbone;

 Compute the pairwise relative transformations $\mathbf{T}_{k,l}$ and the docking confidence scores $w_{k,l}$; **for** $iter = 1$ **to** 4 **do** Compute the absolute transformations $\mathbf{T}_k = (\mathbf{R}_k, \mathbf{t}_k)$ for all $1 \leq k \leq M$ using the transformation synchronization module described in Algorithm 2; Update the graph \mathcal{G}_k based on the current estimate of $\{\mathbf{R}_k, \mathbf{t}_k\}$;

Compute the loss based on the updated transformations and the desired outcome (during training);

return the optimized transformations $T^*(\mathbf{R}_k, \mathbf{t}_k)$;**End Function**

Algorithm 2: Transformation Synchronization Module

Input: $F(w_{k,l}, \mathbf{T}_{k,l}), \forall (k,l) \in \mathcal{E}$ **Output:** $T^*(\mathbf{R}_k, \mathbf{t}_k), \forall k \in \mathcal{V}$ **Function** SYNC(F): Compute the weighted connection Laplacian \mathbf{L} and vector \mathbf{b} ; Calculate the first three eigenvectors \mathbf{U} of \mathbf{L} ; Perform Singular Value Decomposition (SVD) on blocks of \mathbf{U} to obtain $\{\mathbf{R}_k, 1 \leq k \leq N\}$; Solve the synchronization problem defined in Equation (12) to obtain $\{\mathbf{t}_k, 1 \leq k \leq N\}$; **return** $\mathbf{T}_k = (\mathbf{R}_k, \mathbf{t}_k), 1 \leq k \leq M$;**End Function**

B.2 Dataset

The overview of datasets is in Table 1. DIPS is downloaded from <https://github.com/drorlab/DIPS>. The DIPS dataset (Distant Interacting Protein Structures) [18] is constructed by mining the Protein Data Bank (PDB) and serves as a comprehensive collection of protein complex structures where individual protein structures are unavailable. The dataset comprises a curated set of 42,462 binary protein interactions. For this study, we utilized the latest version of the PDB, which provides a total of 282,076 PDB files. To filter the data, we applied the following criteria: a) a buried surface area of more than 500, b) a resolution of NMR structures less than 3.5, c) a sequence identity of less than 30, and d) a complex size exceeding 50.0. The raw PDB files underwent several preprocessing steps as follows:

- Valid residues were identified based on the presence of "Natom," "alphaCatom," and "Catom" attributes.
- The coordinates of the "alphaCatom" were extracted to obtain the residue coordinates.
- Pairwise distances between residues in the two protein arrays were computed. If the distance between residues was less than 8.0, the residues were marked as pockets. Additionally, the pocket ground truth was obtained by averaging the coordinates of the identified pockets from the two proteins.

After performing the above steps, we grouped the docked protein chains with the same PDB and performed subgraph mining on them as shown in Figure 6 to obtain the multibody complexes.

B.3 Data representation

We follow previous work [50, 44] to represent protein as a graph. We construct the graph using the K-nearest neighbors (KNN) graph construction method. We adopt the feature construction used in [44] for feature encoding.

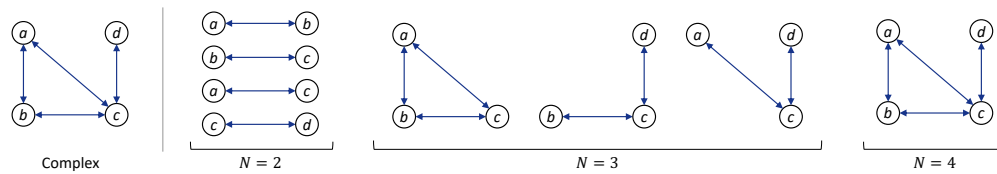


Figure 6: An example of our use of the dataset was obtained by curating from the DIPS dataset: we searched through the proteins to obtain connected subgraphs of different degrees